Transition Met Chem (2013) 38:659–664
DOI 10.1007/s11243-013-9734-4

Synthesis, structure, and conformational mobility of a vaulted *trans*-bis(*o*-aminophenolato)platinum(II) complex

**Naruyoshi Komiya · Koichi Takahashi ·
Tomoya Tanaka · Atsushi Yoshida ·
Takeshi Naota**

Received: 25 April 2013 / Accepted: 17 May 2013 / Published online: 1 June 2013

Abstract The synthesis, structure, and conformational mobility of a *trans*-bis(aminophenolato)platinum(II) complex bearing a dodecamethylene bridge, [Pt(L)] (**1**) [**H_2L** = *N*,*N*′-Dimethyl-*N*,*N*′-bis(2-hydroxyphenylmethyl)dodecane-1,12-diamine] are described. The 2D NMR and X-ray diffraction analysis revealed that the complex has a "reversed U"-shaped *syn* conformation in the solution state, which is mainly due to steric congestion of the vaulted structure and hydrogen bonding at the bis[(*o*-aminomethyl)phenolato] coordination site, while the complex unit is packed in the crystalline state with "Z-shaped" *anti*-conformation due to highly regulated molecular arrangement by 3D CH-π and hydrogen bonding interactions.

Introduction

Transition metal complexes vaulted with carbon chains have been extensively studied as a new candidate for functional materials due to their specific 3D superstructure around bridged ligands and coordination planes [1–3]. Various vaulted complexes have been obtained by the reaction of transition metals with a variety of tether-linked ligands [4–21], and their specific functions have been studied in view of their inclusion properties [7, 9], molecular aggregation [11, 12], optical properties [8, 12–14], and catalytic activity for asymmetric transformation [4–6, 19, 21].

As part of our program aimed at developing new functionalities of flexible *trans*-ligating complexes with highly controllable d-π conjugation, the dynamic behavior of vaulted *trans*-ligating d^8 transition metal complexes with phenolato ligands-bearing *o*-imino [11–14] and *o*-NHC [18] groups have been investigated. In this work, a novel vaulted form of *trans*-bis[(*o*-aminomethyl)phenolato] Pt(II) complex **1** was synthesized. Bis[(*o*-aminomethyl)phenolato] transition metals are an interesting platform for vaulted structures because their small d-π conjugation provides significant molecular mobility due to enhanced flexibility of the metal platform. *Cis*-ligating complexes **2** of Cu(II) [22, 23], Pd(II) [24], Ni(II) [25], and *trans* Pd(II) complexes **3** [26–28] have been reported for this doubly ligating platform, although Pt(II) complexes are limited to mono-ligating complexes **4** with dichloro [29] and chloropyridine [30] ligands (Scheme 1). Complexes **2**–**4** were studied with respect to their chemical [22, 24–28, 30] and biological [23, 29] activities. This is the first example of vaulted bis[(*o*-aminomethyl)phenolato]metal complexes, and also, the first bis[(*o*-aminomethyl)phenolato)] Pt(II) complex. The 2D NMR and X-ray diffraction (XRD) studies revealed that complex **1** has "reversed U"-shaped *syn* conformation in solution, while the packing unit **1** in the crystalline state has a contrastingly "Z"-shaped *anti*-conformation. The molecular flexibility of **1** is clearly distinct from that of *o*-iminophenolato and *o*-NHC-phenolato analogs **5** [13, 14] and **6** [18], which have much more rigid planar and *syn* platforms, respectively, due to enhanced d-π conjugation. This paper describes the synthesis, structure, and dynamic behavior of complex **1**, with

N. Komiya (✉) · K. Takahashi · T. Tanaka · A. Yoshida ·
T. Naota (✉)
Department of Chemistry, Graduate School of Engineering
Science, Osaka University, Machikaneyama, Toyonaka,
Osaka 560-8531, Japan
e-mail: komiya@chem.es.osaka-u.ac.jp

T. Naota
e-mail: naota@chem.es.osaka-u.ac.jp

Scheme 1 Structures of 1–6

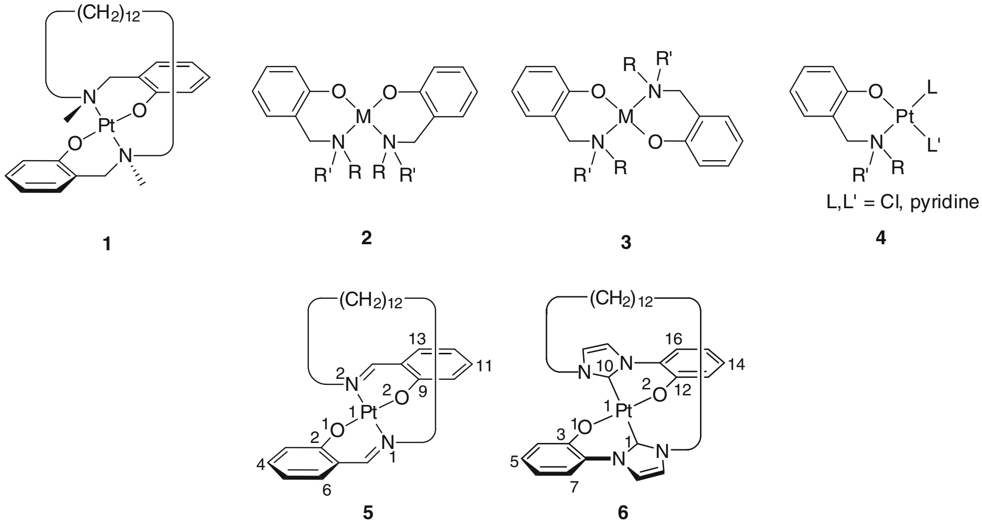

specific focus on the molecular mobility in the solution and crystalline states.

Experimental section

All chemicals were commercially available and used as received without further purification. Melting points were measured in a glass capillary on a Büchi B-545 melting point apparatus. Mass spectra were obtained on a JEOL JMS-DX 303. IR spectra were recorded on a Bruker EQUINOX55/S spectrometer. ^{1}H and ^{13}C NMR spectra were recorded on a Varian Unity-Inova 500 spectrometer. X-ray analysis was carried out on a Rigaku R-AXIS RAPID imaging plate diffractometer with graphite monochromated MoKα radiation.

Preparation of *N*,*N'*-bis(ethoxycarbonyl)dodecane-1,12-diamine

A mixture of 1,12-diaminododecane (4.01 g, 20.1 mmol) and ethyl chloroformate (5.43 g, 50.1 mmol) in pyridine (40 mL) was refluxed at 100 °C for 13 h. After cooling to room temperature, the mixture was poured into water (100 mL) and extracted with ethyl acetate (100 mL). The organic layer was washed successively with a saturated Na_2CO_3 aqueous solution (100 mL × 1), 2 N HCl (100 mL × 3), and water (100 mL × 1), and dried over $MgSO_4$. After filtration, the residue was evaporated under reduced pressure to give *N*,*N'*-bis(ethoxycarbonyl)dodecane-1,12-diamine (3.35 g, 49 %) as a colorless solid. ^{1}H NMR ($CDCl_3$, 500 MHz): δ 1.17–1.35 (m, 22 H), 1.42–1.53 (m, 4 H), 3.16 (q, $J = 6.3$ Hz, 4 H, NCH_2CH_2–), 4.10 (q, $J = 6.7$ Hz, 4 H, CH_3CH_2O–), 4.61 (br, 2 H, N*H*).

Preparation of *N*,*N'*-dimethyldodecane-1,12-diamine

A mixture of *N*,*N'*-bis(ethoxycarbonyl)dodecane-1,12-diamine (2.30 g, 6.68 mmol) and $LiAlH_4$ (1.59 g, 42.0 mmol) in dry THF (50 mL) was refluxed for 24 h. After cooling to 0 °C, excess $LiAlH_4$ was quenched by adding $Na_2SO_4{\cdot}10H_2O$ (9.09 g, 28.2 mmol). Filtration followed by evaporation under reduced pressure gave *N*,*N'*-dimethyldodecane-1,12-diamine (1.42 g, 93 %) as a colorless solid. ^{1}H NMR ($CDCl_3$, 500 MHz): δ 1.23–1.35 (m, 14 H), 1.48 (tt, $J = 7.1$, 7.1 Hz, 4 H, N-$CH_2CH_2CH_2$), 1.63–1.74 (m, 4 H), 2.43 (s, 6 H, NCH_3), 2.56 (t, $J = 7.1$ Hz, 4 H, NCH_2CH_2–); ^{13}C NMR ($CDCl_3$, 125 MHz): δ 27.3, 29.6, 29.9, 30.1, 36.5, 52.2, 62.6.

Preparation of $\mathbf{H_2L}$

A mixture of *N*,*N'*-dimethyldodecane-1,12-diamine (23.4 mg, 0.11 mmol), salicylaldehyde (25.0 g, 0.20 mmol), and $NaBH_3CN$ (15.2 mg, 0.24 mmol) in methanol (4.0 mL) was stirred at 20 °C for 17 h. The mixture was poured into CH_2Cl_2 (20 mL) and extracted with 1 N HCl (20 mL × 2). After the acidity of the solution was adjusted to pH 12 by adding NaOH, the mixture was extracted with CH_2Cl_2 (30 mL). The organic layer was dried over $MgSO_4$, filtered, and evaporated under reduced pressure to give $\mathbf{H_2L}$ (25 mg, 58 %) as an orange oil: ^{1}H NMR ($CDCl_3$, 500 MHz): δ 1.20–1.34 (m, 16 H), 1.54 (tt, $J = 7.2$, 7.2 Hz, 4 H, N-$CH_2CH_2CH_2$), 2.26 (s, 6 H, N-CH_3), 2.46 (t, $J = 7.2$ Hz, 4 H, N-CH_2CH_2), 3.68 (s, 4 H, Ar-CH_2-N), 6.76 (ddd, $J = 7.4$, 7.4, 1.1 Hz, 2 H, H^4), 6.81 (dd, $J = 7.7$, 1.1 Hz, 2 H, H^6), 6.95 (dm, $J = 7.4$ Hz, 2 H, H^3), 7.15 (ddd, $J = 7.7$, 7.4, 1.7 Hz, 2 H, H^5); ^{13}C NMR ($CDCl_3$, 125 MHz): δ 26.9, 27.1, 29.42, 29.45, 29.50, 41.1, 57.1, 61.5, 115.9, 118.8, 122.0, 128.3, 128.5, 158.1; HRMS (EI+): m/z $[M]^+$ calcd for $C_{28}H_{44}N_2O_2$: 440.3403; found: 440.3389.

Preparation of [Pt(L)] (**1**)

A mixture of $PtCl_2(CH_3CN)_2$ (0.351 g, 1.01 mmol), **H_2L** (0.462 g, 1.05 mmol), and K_2CO_3 (1.02 g, 7.38 mmol) in toluene (120 mL) and dimethylsulfoxide (30 mL) was stirred at 140 °C for 24 h under argon atmosphere. After evaporation of the solvent under reduced pressure, the residual oil was diluted with ethyl acetate (100 mL). The organic layer was washed successively with 1 N HCl (50 mL × 2) and water (100 mL) and dried over $MgSO_4$. After filtration and evaporation, the crude orange solid was subjected to column chromatography (SiO_2, *n*-hexane/ethyl acetate = 5:1) to give [Pt(L)] (**1**) (27.8 mg, 4.4 %) as a yellow solid: mp 197.0–198.0 °C; IR (KBr): 3028, 2927, 2855, 1595, 1568, 1478, 1271, 1109, 1035, 883, 794, 763, 726, 614 cm^{-1}; ^1H NMR ($CDCl_3$, 500 MHz): δ 1.26–1.53 (m, 16 H) 2.12–2.26 (m, 4 H), 2.65 (s, 6 H, N-CH_3), 2.91 (d, $J = 11.6$ Hz, 2 H, Ar-CH_aH_b-N), 3.15 (dddd, $J = 16.2, 12.4, 11.7, 5.9$ Hz, 2 H, $ArCH_2NCH_2CH_aH_b$), 3.49 (ddd, $J = 12.4, 12.4, 5.1$ Hz, 2 H, N-$CH_aH_bCH_2$), 4.16 (d, $J = 11.6$ Hz, 2 H, Ar-CH_aH_b-N), 6.59 (ddd, $J = 7.3, 7.3, 0.9$ Hz, 2 H, H^4), 6.72 (dd, $J = 7.9, 0.9$ Hz, 2 H, H^6), 6.94 (dd, $J = 7.3, 1.8$ Hz, 2 H, H^3), 7.06 (ddd, $J = 7.9, 7.3, 1.8$ Hz, 2 H, H^5); ^{13}C NMR ($CDCl_3$, 125 MHz): δ 24.7, 25.90, 25.94, 26.9, 27.5, 49.2, 61.2, 63.4, 116.3, 117.9, 125.6, 130.0, 130.3, 167.6; HRMS (FAB^+): m/z calcd for $C_{28}H_{42}N_2O_2{}^{195}Pt$ $(M)^+$: 633.2894; found: 633.2894.

X-ray structure determination

Crystal suitable for XRD study was analyzed by using a Rigaku R-AXIS RAPID imaging plate diffractometer with graphite-monochromated MoKα radiation ($\lambda = 0.71075$ Å). The structure of complex **1** was solved by direct methods and refined by the full-matrix least-square method. In the subsequent refinement, the function $\Sigma\omega(F_o^2 - F_c^2)^2$, in which F_o and F_c were the observed and calculated structure factor amplitudes, respectively, was minimized. The positions of non-hydrogen atoms were found from difference Fourier electron density maps and refined anisotropically. All calculations were performed using crystal structure crystallographic software package. Details of the structure determinations are given in Fig. 1 and Table 1.

Computational methods

All calculations were carried out based on the density functional theory (DFT) with the B3LYP exchange–correlation functional [31], using the Spartan 10 program package (Wavefunction, Inc., Irvine, CA). The basic set used was the effective core potential for platinum atom [32] and 6-31G* for the remaining atoms [33].

Results and discussion

Complex **1** was prepared by the reaction of $PtCl_2(CH_3CN)_2$ with **H_2L** (1 equiv) and K_2CO_3 (7 equiv) in toluene/

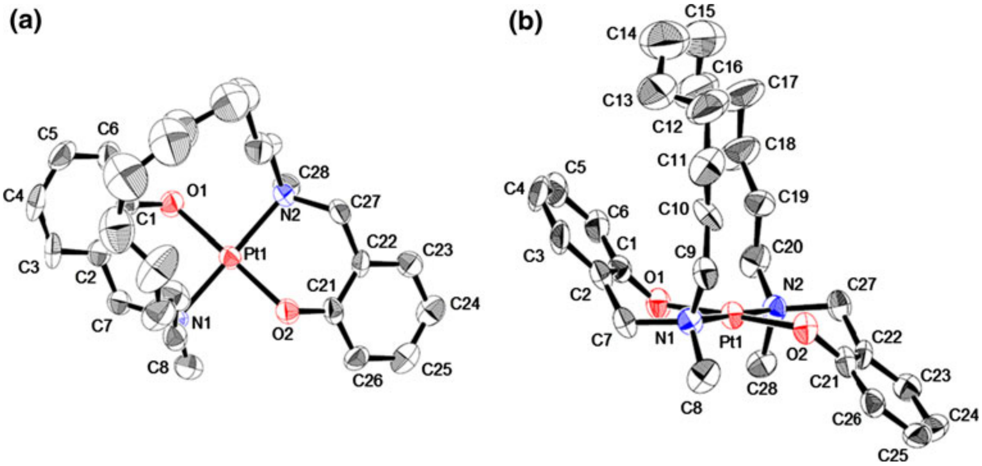

Fig. 1 ORTEP drawing of complex **1**. **a** *Top view*. **b** *Side view*. Thermal ellipsoids are shown at the 30 % probability level. Hydrogen atoms are omitted for clarity. Selected bond distances (Å) and angles (°): Pt(1)–O(1), 2.021(8); Pt(1)–O(2), 2.017(8); Pt(1)–N(1), 2.065(9); Pt(1)–N(2), 2.074(9); O(1)–Pt(1)–O(2), 179.3(3); N(1)–Pt(1)–N(2), 179.5(4); N(1)–Pt(1)–O(1)–C(1), 42.3(6); N(2)–Pt(1)–O(2)–C(21), 39.5(6); O(1)–Pt(1)–N(1)–C(7), 7.3(6); O(2)–Pt(1)–N(2)–C(27), 10.3(6); N(1)–C(7)–C(2)–C(1), 60.8(13); N(2)–C(27)–C(22)–C(21), 60.7(12)

Table 1 Crystal data and structure refinement details for compound **1**

Formula	$C_{28}H_{42}N_2O_2Pt$
Formula weight	633.74
Temperature (K)	293
Crystal size (mm)	0.20 × 0.20 × 0.02
Crystal system	Monoclinic
Space group	$P2_1/c$ (#14)
a (Å)	19.561(2)
b (Å)	9.7112(6)
c (Å)	14.467(1)
α (°)	90
β (°)	100.241(1)
γ (°)	90
V (Å^3)	2704.4(4)
Z value	4
D_{calcd} (gcm^{-3})	1.556
μ(MoKα) (mm^{-1})	5.194
F(000)	1272.00
$2\theta_{max}$ (°)	54.8
No. of reflections measured	52780
No. of observed reflections	6130
No. of variables	298
R_1 [$I > 2\sigma(I)$][a]	0.080
wR_2 (all reflections)[b]	0.144
Goodness of fit	1.11

[a] $R_1 = \Sigma(|F_o|-|F_c|)/\Sigma(|F_o|)$

[b] $wR_2 = [\Sigma[w(F_o^2-F_c^2)^2]/\Sigma w(F_o^2)^2]^{1/2}$

dimethyl sulfoxide (4:1) at 140 °C. Ligand $\mathbf{H_2L}$ was prepared from 1,12-diaminododecane in three steps (Scheme 2). Complex **1** was characterized by spectroscopic methods including H–H correlation spectroscopy (COSY) and nuclear Overhauser effect spectroscopy (NOESY).

Trans-coordination and vaulted structures of **1** have been unequivocally established from XRD analysis of a crystal obtained by recrystallization from hexane/AcOEt (Table 1). An ORTEP drawing of **1** is shown in Fig. 1. Complex **1** has *anti*-conformation, where the dihedral angles between the coordination plane [Pt(1)–O(1)–N(1)/Pt(1)–O(2)–N(2)] and aromatic plane [C(1)–C(3)–C(5)/C(21)–C(23)–C(25)] are 43.8° and 39.3°, respectively (Fig. 1b). Large torsion angles of [N(1)–Pt(1)–O(1)–C(1)] (42.3°) and [N(2)–Pt(1)–O(2)–C(21)] (39.5°) indicate that the bent structure is mainly due to folding along the lines O(1)–C(7) and O(2)–C(27). Intraligand H-bonding interactions between phenoxy oxygen atoms O(1)/O(2) and linker protons H(20a)/H(9b) are observed with H-bonding distance of 2.41 and 2.73 Å. Noteworthy is strong contact between H(10a) and C(2) with sufficiently short distance of 2.44 Å, which indicates that the unprecedented *anti*-conformation of **1** in the crystalline state is partially the result of intramolecular CH-π interactions between linker hydrogen and aromatic planes. The dodecamethylene-vaulted analogs of bis(*o*-iminophenoxy) and bis(*o*-NHC-phenoxy) platinum(II) complexes **5** [13, 14] and **6** [18] have contrastingly planar and *syn* conformations, respectively, as shown in Fig. 2.

The ^{1}H NMR (500 MHz) spectrum of **1** in $CDCl_3$ at 298 K has one set of aromatic protons H(3), H(4), H(5), and H(6) in the range of 6.57–7.07 ppm, which indicates that the complex has symmetrical conformation in the solution state (Fig. 3). Clear splitting and a significant downfield shift of H(7b)/H(27b) protons at 4.16 ppm indicate that these protons undergo intraligand H-bonding interactions with O(1)/O(2), which are similar to those in the crystalline state. A strong remote correlation in the NOESY (500 MHz) spectrum is observed between *N*-methyl H(8) and aromatic H(6) protons on the other side of the aromatic region (correlation A in Fig. 3), in

Scheme 2 Synthetic route for [Pt(L)] **1**

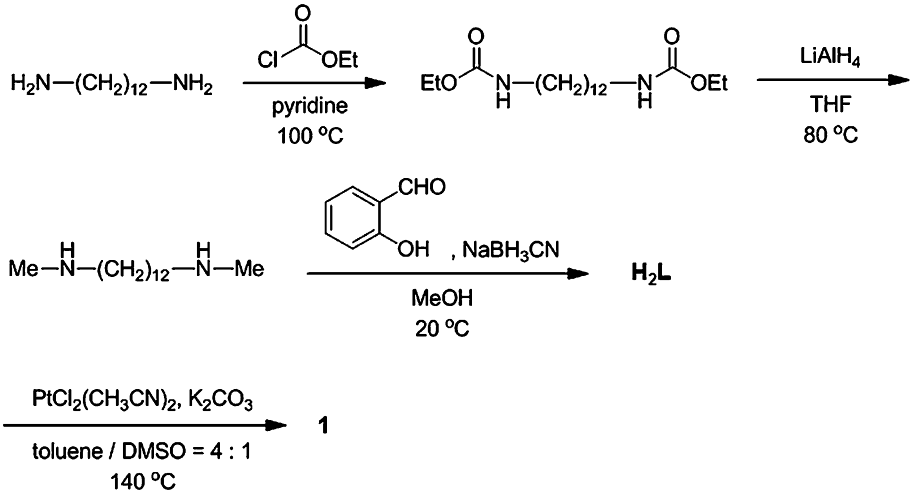

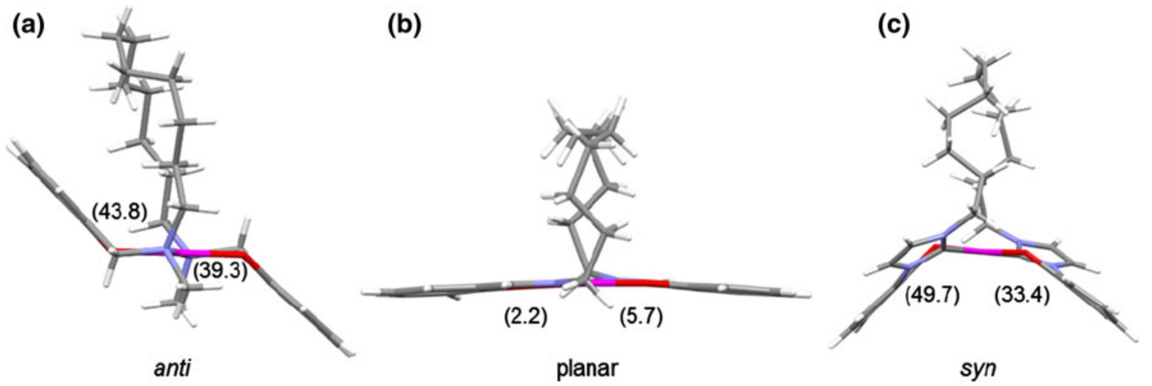

Fig. 2 Contrasting conformations of dodecamethylene-vaulted platinum(II) complexes **1** (**a**), **5** [13, 14] (**b**), and **6** [18] (**c**) determined by single crystal XRD. Values in parentheses are dihedral angles between the coordination and aromatic planes. Coordination planes: [Pt(1)–O(1)–N(1)/Pt(1)–O(2)–N(2)] for **1**; [Pt(1)–O(1)–N(1)/Pt(1)–O(2)–N(2)] for **5**; [Pt(1)–O(1)–C(1)/Pt(1)–O(2)–C(10)] for **6**. Aromatic planes: [C(1)–C(3)–C(5)/C(21)–C(23)–C(25)] for **1**; [C(2)–C(4)–C(6)/C(9)–C(11)–C(13)] for **5**; [C(3)–C(5)–C(7)/C(12)–C(14)–C(16)] for **6**. Numbering of the atoms for these structures is shown in Fig. 1 for **1** and Scheme 1 for **5** and **6**

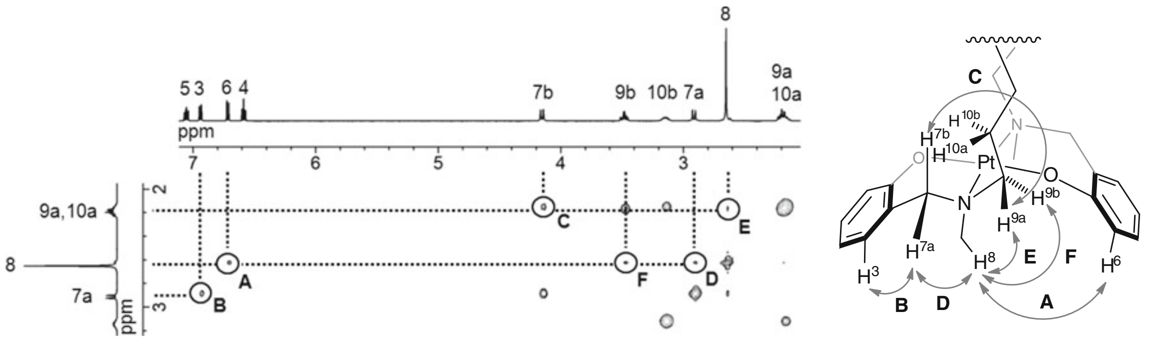

Fig. 3 ^{1}H NMR/NOESY (500 MHz) spectra and the major NOE correlation of **1** in $CDCl_3$ (298 K, mixing time = 0.700 s)

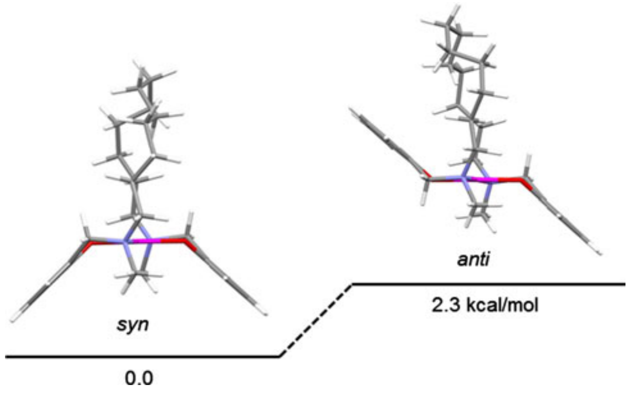

Fig. 4 Optimized structure and relative energy for *syn*- and *anti*-**1** in gas phase estimated by DFT calculations (B3LYP/LACVP*) based on the geometries of the *anti*-form obtained from single crystal XRD

addition to expected correlations of H(3)–H(7a) (B), H(7b)–H(9a) (C), H(7a)–H(8) (D), H(8)–H(9a) (E), and H(8)–H(9b) (F). This indicates that complex **1** has rigid *syn* conformation in the solution state, which is in contrast to the *anti*-conformation in the crystalline state (Fig. 1b) DFT calculations (B3LYP/LACVP*) based on the optimized structure in gas phase indicate that the *syn* conformation of **1** is more stable than the *anti*-conformation by 2.3 kcal/mol (Fig. 4). The rigid *syn* conformation of **1** in the solution state can be ascribed to the steric repulsion around the aromatic moiety and molecular constraint caused by hydrogen bonding at H(7b)/H(27b)–O(1)/O(2) and H(9b)/H(20a)–O(2)/O(1).

The molecular packing of crystal **1** is shown in Fig. 5. The most important feature evident in this crystal is the herringbone packing motif, which consists of intermolecular hydrogen bonding between aromatic protons and phenoxy oxygens [H(3)–O(2) (2.68 Å, broken line A), H(23)–O(1) (2.51 Å, B)]. Intermolecular [H(8a)–C(25) (2.93 Å, broken line C), H(20b)–C(5) (2.89 Å, D)] and intramolecular [H(10a)–C(2) (2.44 Å)] CH-π interactions are also observed between methyl/methylene protons and aromatic ring. Therefore, the *anti*-form of the molecular unit is the result of sufficient stabilization achieved by these inter- and intra-molecular interactions in the crystalline state, although this is thermodynamically unfavorable in the solution state. Such dynamic molecular

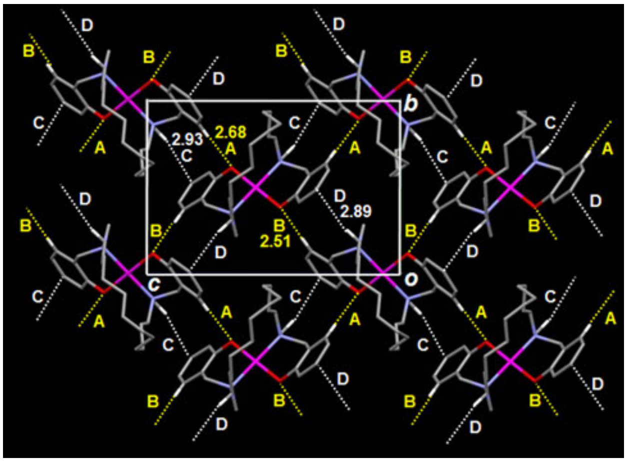

Fig. 5 Packing of **1**. *a*-Axis projection showing hydrogen bonding (*broken lines*, *A* and *B*) and CH-π (*broken lines*, *C* and *D*) interactions

movement observed in the solution and crystalline states would be due to the valance of weak d-π conjugation of the bis[(*o*-aminomethyl)phenolato] coordination site and corresponding molecular constraint of the vaulted structure.

Conclusions

In summary, we have synthesized the first vaulted *trans*-bis(*o*-aminomethylphenolato)Pt(II) complex **1** bearing a polymethylene bridge. The flexible coordination plane with weak d-π conjugation generates bistability for *syn* and *anti*-conformations in the solution and crystalline states, respectively. Further research is currently underway to apply the related vaulted complexes with high flexibility as new functional materials.

Supplementary materials

CCDC 937955 contains the supplementary crystallographic data for **1**. These data can be obtained free of charge from The Cambridge Crystallographic Data Centre via www.ccdc.cam.ac.uk/data_request/cif.

Acknowledgments This work was supported by Grant-in-Aid for Scientific Research, from the Ministry of Education, Culture, Sports, Science and Technology, Japan.

References

1. Boschi T (1994) In: Montanari F, Casella L (eds) Metalloporphyrins catalyzed oxidations. Kluwer Academic Publishers, Dordrecht, pp 239–267
2. Skopek K, Hershberger MC, Gladysz JA (2007) Coord Chem Rev 251:1723–1733
3. Ito Y, Kuwano R (1999) Phosphorus Sulfur Silicon Relat Elem 144–146:469–472
4. Groves JT, Viski P (1989) J Am Chem Soc 111:8537–8538
5. Naruta Y, Tani F, Ishihara N, Maruyama K (1991) J Am Chem Soc 113:6865–6872
6. Collman JP, Zhang X, Hembre RT, Brauman JI (1990) J Am Chem Soc 112:5356–5357
7. Lexa D, Momenteau M, Savéant JM, Xu F (1986) J Am Chem Soc 108:6937–6941
8. Ikai M, Ishikawa F, Aratani N, Osuka A, Kawabata S, Kajioka T, Takeuchi H, Fujikawa H, Taga Y (2006) Adv Funct Mater 16:515–519
9. Takeuchi KJ, Busch DH, Alcock N (1983) J Am Chem Soc 105:4261–4270
10. Hendrickson AR, Hope JM, Martin RL (1979) J Chem Soc Dalton Trans 1497–1502
11. Naota T, Koori H (2005) J Am Chem Soc 127:9324–9325
12. Komiya N, Muraoka T, Iida M, Miyanaga M, Takahashi K, Naota T (2011) J Am Chem Soc 133:16054–16061
13. Komiya N, Okada M, Fukumoto K, Jomori D, Naota T (2011) J Am Chem Soc 133:6493–6496
14. Komiya N, Okada M, Fukumoto K, Kaneta K, Yoshida A, Naota T (2013) Chem Eur J 19:4798–4811
15. Bailey NA, Barrass A, Fenton DE, Gonzalez MSL, Moody R, Rodriquez de Barbarin CO (1984) J Chem Soc Dalton Trans 2741–2746
16. Khandar AA, Cardin C, Hosseini-Yazdi SA, McGrady J, Abedi M, Zarei SA, Gan Y (2010) Inorganica Chim Acta 363:4080–4087
17. Goto H, Hayakawa T, Furutachi K, Sugimoto H, Inoue S (2012) Inorg Chem 51:4134–4142
18. Komiya N, Yoshida A, Naota T (2013) Inorg Chem Commun 23:122–126
19. Sawamura M, Hamashima H, Ito Y (1992) J Am Chem Soc 114:8295–8296
20. Jung M, Suzaki Y, Saito T, Shimada K, Osakada K (2012) Polyhedron 40:168–174
21. Zhang X, Qin Y, Rao B, Luo M (2009) Organometallics 28:3093–3099
22. Guo YM, Du M, Wang GC, Bu XH (2002) J Mol Struct 643:77–83
23. Storr T, Merkel M, Song-Zhao GX, Scott LE, Green DE, Bowen ML, Thompson KH, Patrick BO, Schugar HJ, Orvig C (2007) J Am Chem Soc 129:7453–7463
24. Mohanty S, Suresh D, Balakrishna MS, Mague JT (2009) J Organomet Chem 694:2114–2121
25. Rotthaus O, Thomas F, Jarjayes O, Philouze C, Saint-Aman E, Pierre JL (2006) Chem Eur J 12:6953–6962
26. Grigor BA, Nielson AJ (1977) J Organomet Chem 129:C17–C18
27. Valk JM, van Belzen R, Boersma J, Spek AL, van Koten G (1994) J Chem Soc Dalton Trans 2293–2302
28. Ghorai D, Mani G (2011) Inorganica Chim Acta 372:412–416
29. Wasi N, Singh HB (1987) Inorganica Chim Acta 135:133–137
30. Shimazaki Y, Yajima T, Nakabayashi Y, Naruta Y (2009) Inorganica Chim Acta 362:887–893
31. Becke AD (1995) In: Yarkony DR (ed) Modern electronic structure theory part II. World Scientific, Singapore, pp 1022–1046
32. Hay PJ, Wadt WR (1985) J Chem Phys 82:270–283
33. Francl MM, Pietro WJ, Hehre WJ, Binkley JS, Gordon MS, DeFrees DJ, Pople JA (1982) J Chem Phys 77:3654–3665